Tracking coarse sediment in an Alpine subglacial channel using radio-tagged particles

Matt Jenkin[1] (ID), Margaux Hofmann[1], Bryn Hubbard[2] (ID), Davide Mancini[1], Floreana M. Miesen[1], Frédéric Herman[1] and Stuart N. Lane[1]

[1]Institute of Earth Surface Dynamics, University of Lausanne, Lausanne, Switzerland and [2]Department of Geography & Earth Sciences, Aberystwyth University, Aberystwyth, UK

Abstract

We present a method for tracking radio-tagged pebbles and cobbles through subglacial meltwater channels under shallow temperate glaciers. Natural particles tagged with active radio transmitters were injected directly into a large subglacial channel 300 m up-glacier from the terminus of the Glacier d'Otemma, Switzerland. A roving antenna was developed to localise tagged particles planimetrically in subglacial and proglacial channel reaches (350 and 150 m long, respectively) using a probabilistic technique, delivering records of the change in particle location and transport distance over time with uncertainty. The roving antenna had a ±5−15 m planimetric precision, a 75% particle localisation rate and operated at a maximum ice depth of 47 m. Additionally, stationary supraglacial and proglacial antennas continuously monitored the passage of tagged particles through consecutive reaches of the channel, constraining the timing of particle transport events. The proglacial antenna system had a 98.1% detection rate and was operational to 0.89 m water depth during testing. Roving and stationary antenna records were combined to create a transport distance model for each particle, which may be used in conjunction with hydraulic data to investigate the kinematics of particle motion. When applied at scale in future studies, this method may be used to reveal the mechanisms and timescales of coarse sediment export from Alpine glaciers.

1. Introduction

Temperate Alpine glaciers erode significant quantities of sediment as they slide over their beds (Hallet, 1979, 1996; Cook and others, 2020; Herman and others, 2021). Much of this eroded material is exported from the glacier by meltwater flowing through the subglacial drainage network (Alley and others, 1997; Koppes and others, 2015; Alley and others, 2019) and is a primary source of sediment supplied to downstream environments, exerting a major control on the formation and evolution of glacial land-systems (Jaeger and Koppes, 2015). Glacial erosion rates and downstream sediment yields are expected to change as glaciers recede in a warming climate (Lane and others, 2017; Delaney and Adhikari, 2020; Herman and others, 2021) and are commonly estimated using measurements of suspended sediment load in proglacial rivers (e.g. Riihimaki and others, 2005; Swift and others, 2005; Koppes and Montgomery, 2009; Herman and others, 2015). Recent field and modelling studies (e.g. Beaud and others, 2018a; Perolo and others, 2019) challenge the assumption that eroded sediment is rapidly evacuated by meltwater (e.g. Alley and others, 1997), which has important implications for the use of proglacial sediment export measurements as a reliable proxy for glacial erosion and sediment yield over time. The problem remains that very little is known about when and under what conditions a glacier margin evacuates the sediment supplied to it. This is particularly the case for bedload transport, which is extremely difficult to quantify.

Particle tracking techniques that follow individual pebbles or cobbles using radio-frequency identification (RFID) tags have been widely used to investigate coarse sediment transport dynamics in rivers (e.g. Lamarre and others, 2005; Bradley and Tucker, 2012; Liébault and others, 2012; Hassan and Roy, 2016; Cassel and others, 2017). In general, particles are tagged with radio transponders or transmitters that emit signals containing a unique ID code that are received by roving or stationary antennas, permitting the geolocation of individual particles at a given time. However, tracking techniques have not yet been applied in subglacial channels, primarily due to the lack of an RFID system that is practically scalable for use with hundreds to thousands of subglacially deployed particles. Such a system must have a detection range sufficient to observe particles submerged in meltwater flowing beneath tens of metres of heterogeneous glacier ice, an extended operational life and a reliable data retrieval method. Wireless sensor platforms developed to obtain hydrological and glaciological measurements of the englacial and subglacial environment (Martinez and others, 2004, 2005; Hart and others, 2006; Bagshaw and others, 2012; Smeets and others, 2012; Bagshaw and others, 2014; Hart and others, 2019; Alexander and others, 2020; Prior-Jones and others, 2021) offer a framework for designing a system optimised for bulk subglacial particle tracking, but their development and mass-production is prohibitively expensive and time-consuming, requiring substantial electronic and mechanical engineering knowledge.

cambridge.org/jog

Alternatively, small, simple and commercially available, active ultra-high frequency (a-UHF), 433 MHz RFID transmitters and receiving antennas have recently been used for particle tracking in rivers (Cassel and others, 2017, 2020, 2021). These RFID systems present an opportunity for tracking large amounts of subglacially deployed radio-tagged particles through shallow ice using receiving antennas located on the glacier surface. This is due to: (1) the high transmit power and correspondingly high detection range enabled by the internal battery in the transmitters ($\sim 60 - 80$ m in air and ~ 2.5 m in water) and (2) the relatively favourable attenuation properties of UHF radio signals in pure, cold glacier ice (Fujita and others, 2000; Barwick and others, 2005; Martinez and others, 2005; Lewis and others, 2015; Hashmi and Brennan, 2022). These off-the-shelf RFID systems have the potential to be rapidly deployed with a minimum of technical radio-systems knowledge.

Here, we present a proof-of-concept for an a-UHF RFID-based particle tracking method to obtain field data on coarse sediment transport in large subglacial channels under shallow temperate glacier ice. Natural particles were tagged with active radio transmitters, injected directly into a major subglacial channel, then tracked in space and time using independent roving and stationary antenna systems. We develop a probabilistic method for localising individual tagged particles with a roving antenna, applying a density estimation technique to point clouds of received radio signals. Compared to existing localisation methods, this has the advantage of being able to accommodate uncertainty estimation, large survey areas with variable survey lines and sparse RFID data. In addition, stationary antennas placed over the subglacial and proglacial channels were used to constrain the particle location to a specific channel reach between roving antenna surveys. Combining these Lagrangian and Eulerian approaches to obtaining information on particle transport (e.g. Ballio and others, 2018), the method can reveal changes in the planimetric position and transport distance of tagged particles over time, with estimated uncertainty. We examine four particles (P1-4) in detail to illustrate the method, drawing from a larger sample of 56 particles injected in a single batch in 2021. This larger sample is used to assess the overall performance of the tracking systems. Ultimately, we assess the advantages, limitations, potential use-cases and scope for development of the method.

1.1. Study area

Method development and testing took place at the Glacier d'Otemma; a large ($14\,\mathrm{km}^2$), temperate valley glacier located in the Valais (Pennine) Alps, Switzerland (Fig. 1). It has an elevation range of 2490–3560 m a.s.l. and three primary accumulation basins that supply a 6.2 km long glacier tongue characterised by a low mean surface gradient (4.8°) and a southwesterly aspect. The tongue is divided by two medial moraines and is partially debris-covered in the lower kilometre. The glacier has undergone 4.1 km of frontal retreat and more than 200 m of ice surface lowering since its Little Ice Age maximum extent *ca.* 1850 and has retreated $\sim 50\,\mathrm{m\,a^{-1}}$ since 2017 (adapted from GLAMOS, 1881–2020). The underlying bedrock, and thus exported sediment, primarily consists of orthogneiss, granodiorite and gabbro (Burri and others, 1999). Ground penetrating radar (GPR), ice surface-lowering and hydraulic potential analyses performed in 2018 were used to locate a single major subglacial channel (~ 10 m wide) under the non-debris-covered zone of the snout-margin, running adjacent to the northern moraine (Egli and others, 2021, 2021b). This channel discharges meltwater and glaciogenic sediment into the Dranse de Bagnes river, which supplies and modifies a $1.6\,\mathrm{km}^2$ glaciofluvial outwash plain (Mancini and Lane, 2020; Müller and others, 2022). The Glacier d'Otemma was selected for this particle tracking study following the recent mapping of the subglacial channel (Egli and others, 2021b). This mapping suggested the presence of a non-pressurised subglacial channel where we wish to understand how sediment moves from under the glacier out into the proglacial margin.
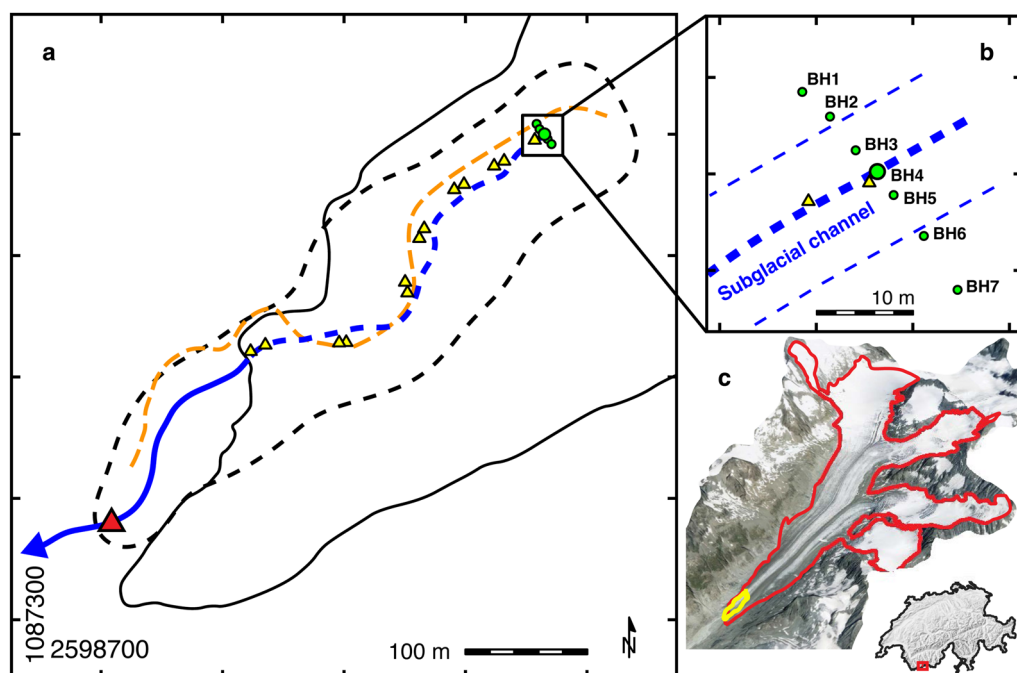

Figure 1. Study area at the Glacier d'Otemma, western Switzerland. (a) Main features of the snout marginal zone: estimated subglacial channel location in 2018 (dashed orange line, adapted from Egli *et al.* 2021b), 2021 channel centreline estimated using particle tracking data (dashed blue line), proglacial channel (solid blue line, arrow indicates flow direction), supraglacial antenna locations (yellow points), the proglacial antenna location (red triangle) and the overall survey zone (dashed black line). (b) Locations of boreholes BH1-7 (green points) relative to the estimated subglacial channel centreline and banks (blue dashed lines). (c) Overview of the Glacier d'Otemma (red line) and the survey zone (yellow line) (Imagery ©2023 Google, CNES/Airbus, Maxar Technologies).

2. Methods

The field data collection and data processing steps in the particle tracking method are subdivided into four primary phases: (1) particle injection, (2) roving antenna surveys, (3) stationary antenna surveys and (4) transport distance modelling (Fig. 2). In phase 1a, natural pebble to cobble-sized particles are tagged with a-UHF RFID transmitters. In phase 1b, the main subglacial channel is accessed through boreholes created using a hot water ice drill 300 m up-glacier of the glacier terminus and tagged particles are injected into the channel. In phase 2, a roving antenna system is used to determine the planimetric position of individual tagged particles on a daily basis, and to estimate their downstream transport distance. Phase 3 involves the use of stationary supraglacial and proglacial antenna arrays to determine whether a tagged particle is located within a given reach of subglacial or proglacial

channel, running concurrently with phase 2. Phase 4 unites the roving and stationary antenna data to produce a transport distance model for each tagged particle. A review of the particle tracking technologies that underpin the methodological approach is provided in the Supplementary Materials. Data analysis was performed using the open-source R programming language for statistical computing. Spatial data were collected and are presented in the Swiss CH1903+/LV95 coordinate reference system.

2.1. Particle injection (1)

2.1.1. Particle tagging (1a)

56 natural, sub-rounded particles of the same rock type as the bedrock underlying the Glacier d'Otemma (orthogneiss), with b-axes between 50 and 100 mm (very coarse pebbles to cobbles),
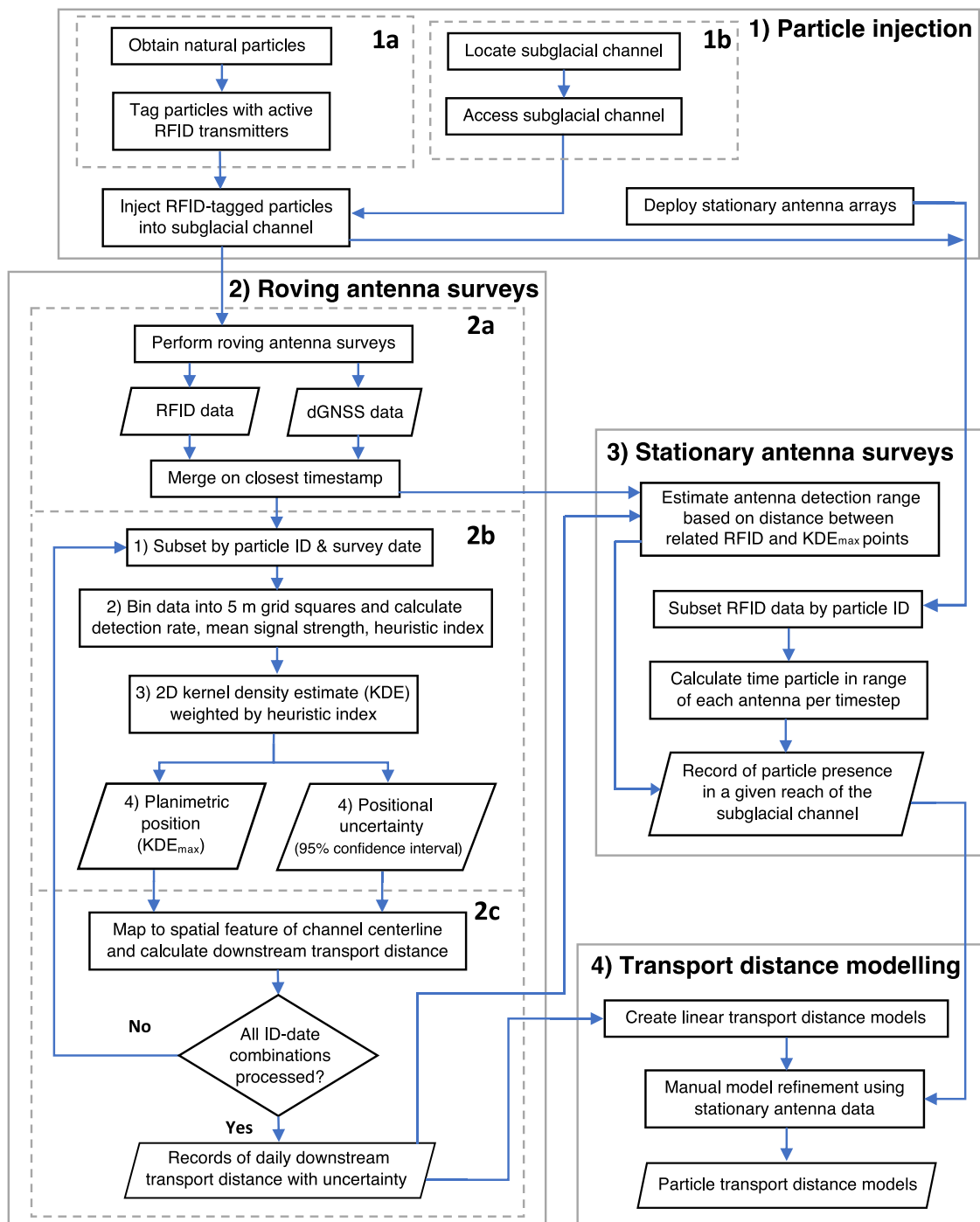

Figure 2. Flowchart of the RFID-tagged particle tracking method.

Figure 3. Tagging natural particles with active RFID transmitters. (a) Cavity creation with a drill press and diamond-tipped core bits. (b) Cross-section and top-down view of pebbles following transmitter insertion.

were tagged with a-UHF RFID tags manufactured by ELA Innovation, Montpellier, France (COIN ID model). Each Ø36 × 11.5 mm, 11 g tag was placed label-side up inside a Ø36 × 25 mm cavity drilled into the particle b-axis using a water-cooled drill press with diamond-tipped core bits manufactured by Diabohr Tech, Germany (Fig. 3). Particles tended to fracture during the cavity excavation if their smallest axis was <5 cm, hence the use of relatively coarse sediment. The tag was sealed in the cavity with a clear two-part epoxy resin ($1.15\,g\,cm^{-3}$), ensuring that it was immersed. Tagging a single particle took 8 minutes on average, excluding curing time. Particles were required to have a density of $2.32–2.98\,g\,cm^{-3}$ after tagging, corresponding to the 3σ range of a sample of 70 untagged natural particles with a mean density of $2.62\,g\,cm^{-3}$. The mean change in particle density caused by tag insertion was −2.6% for this larger sample. The mean density of the 56 particles tracked in this study was $2.61\,g\,cm^{-3}$ after tagging. Each 433 MHz tag was programmed to transmit a −20 dBm radio packet containing a unique

6-character alphanumeric ID code every 200 ms, hereafter referred to as a 'transmission'. This is the fastest programmable transmission interval, chosen to maximise the likelihood of transmission reception at the glacier surface. The tags were powered by internal 3 V lithium CR2032 coin batteries that were insensitive to subglacial temperatures and provided up to 4 months of operational life. The tagged particles were programmed, activated and tested using an ELA PROG IR device immediately before injection into the subglacial channel.

2.1.2. Subglacial channel access and particle injection (1b)

Hot water ice drilling (e.g. Hubbard and others, 1995; Hubbard and Glasser, 2005; Sugiyama and others, 2008; Tsutaki and Sugiyama, 2009; Talalay and others, 2018; Miles and others, 2019) was performed to create boreholes that directly accessed a major subglacial channel at the Glacier d'Otemma. Seven ~Ø15 cm, 47 m deep boreholes (BH1-7) were drilled across a NNW-SSE transect at 2536 m a.s.l., 300 m up-glacier of the channel outlet in late July 2021 (Figs. 1; 4a). Supraglacial meltwater was pumped into a 1000 litre holding tank using a Honda WX15 pump and Ø3/4" PVC hose with a coarse sediment filter, allowing sediments to settle and an uninterrupted water supply to the drill. This water was pressurised to ~110 bar and heated to ~80 °C with Kärcher 9/23G and HD64 units. The water was then passed through a spooled Ø1/2" × 125 m thermoplastic hose (Polyhose PH148-08) mounted to a bespoke, electronically operated winch and sheave wheel system (Fig. 4a) powered by a Honda EG3600CL generator. A custom-built Ø50 mm × 1.2 m, 12.5 kg brass drill stem was attached to the outlet of the hose for stability while drilling. A straight-jet nozzle was attached to the end of the stem to obtain a water throughput of $\sim 17\,l\,min^{-1}$, yielding ~Ø15 cm boreholes at rates of $25–30\,m\,h^{-1}$. A trial attempt to inject particles via englacial moulins in 2020 was unsuccessful because they became trapped in plunge-pool features before reaching the glacier bed for the duration of the melt season (e.g. Bagshaw and others, 2012).

Based on observations made with a 360° GoPro camera inserted into each borehole, BH2 and BH6 accessed the true-right and true-left banks of the channel at peak discharge, respectively, while BH3-5 provided access to the main flow (Fig. 5).
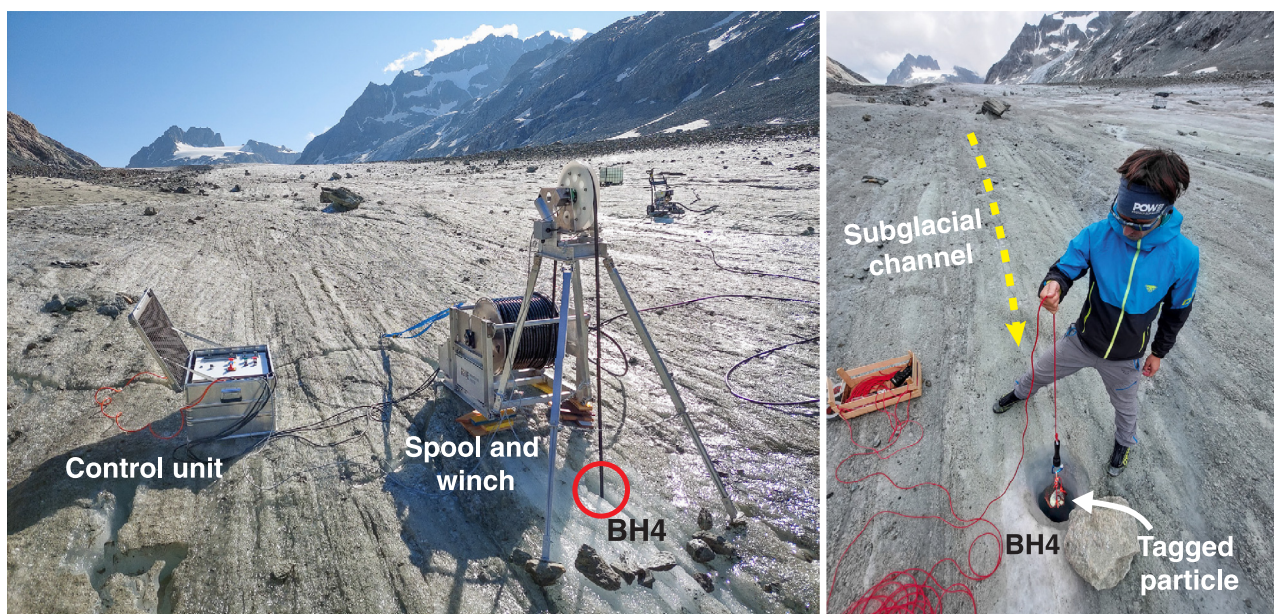

Figure 4. Ice drilling and tagged particle deployment. (a) Hot water ice drill winch system above borehole BH4. (b) Lowering a tagged particle into the subglacial channel via BH4.
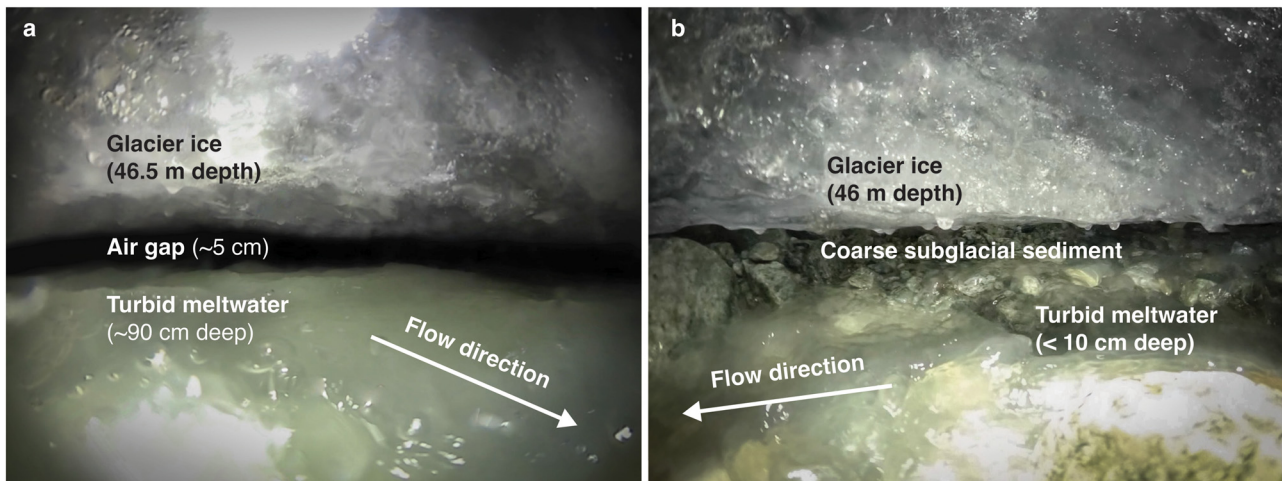
Figure 5. Images of the glacier bed and subglacial channel. (a) Subglacial channel thalweg observed via borehole BH4. (b) True-right bank of the subglacial channel observed via BH2.

Throughout the study, the channel appeared to be non-braided, 10–12 m wide, 0.5–0.9 m deep and non-pressurised with a 5–20 cm air gap even at peak discharge. The channel was located ~15 m south of its 2018 position at this transect. The flow depth and velocity were perceptibly greatest below BH4 which was selected for tagged particle injection. The 56 tagged particles were injected into the channel between 10:00 and 10:20 on 15 August 2021 by lowering them through BH4 in a net attached to the end of a rope (Fig. 4b).

2.2. Roving antenna surveys (2)

2.2.1. Field data collection (2a)

The roving antenna system was developed to survey a 350 m long zone of the glacier snout and a 150 m long reach of the proglacial river for tagged particles, recording the position of the antenna when radio transmissions were received (Fig. 6). The roving antenna consisted of an RFID antenna and reader system manufactured by ELA Innovation, alongside a Trimble R10 differential GNSS (dGNSS) unit, all mounted to a backpack frame (Fig. 6a).

The passive, linearly polarised, semi-directional, half-wavelength RFID antenna (+7 dBi gain ELA Slender III) was connected directly with a coaxial adaptor to an individual RFID reader (SCIEL Reader R) and fixed horizontally to the base of the backpack frame at a height of ~0.7 m above the ground when carried. The reader decoded and validated each received transmission, delivering particle ID code and received signal strength information (RSSI). The readers are capable of detecting multiple tags transmitting simultaneously in the antenna's sensing field. The reader was powered over USB with a Trimble TSC7 controller, which served the dual function of recording and timestamping the reader output using a terminal emulator, as well as simultaneously recording the antenna location at 1 s intervals using Trimble Access software. The mean horizontal precision was ±0.02 m. The dGNSS and RFID logging both utilised the controller clock in GNSS time. The dGNSS beeped when logging, allowing the operator to stop during (extremely rare) signal drop-outs. Following a survey, each received transmission was matched to the point location with the nearest time-stamp, discarding transmissions that could not be matched to a
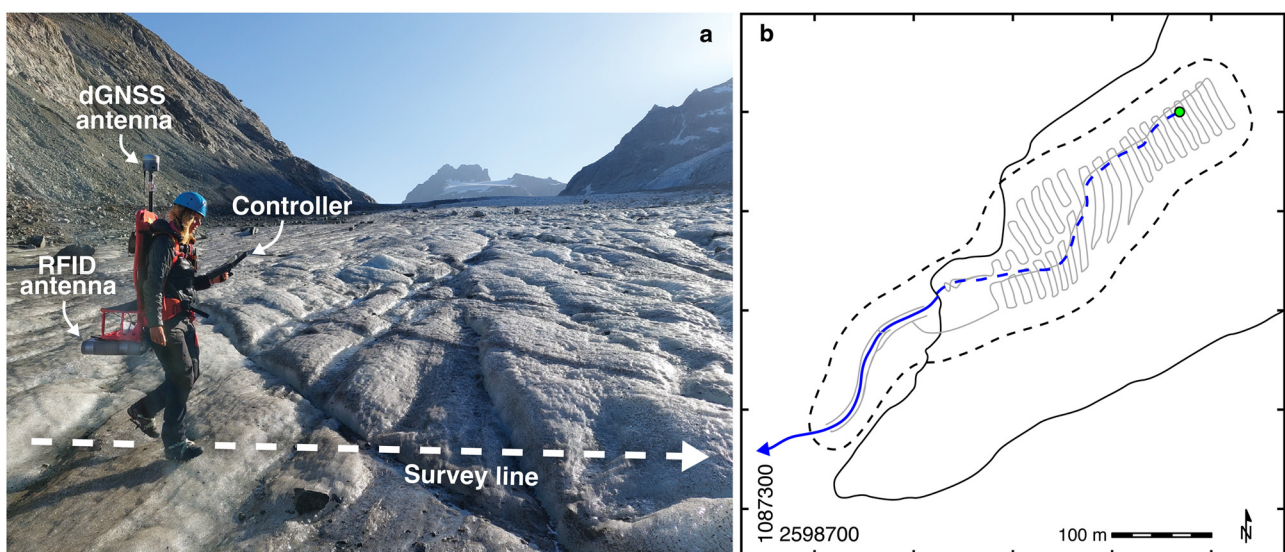

Figure 6. Roving antenna survey. (a) Performing a survey for subglacial RFID-tagged particles. (b) The master survey track (solid grey line) and survey extent (dashed black line) over a reach of the subglacial channel (blue dashed line) and the main proglacial channel (solid blue line). Particle injection location indicated with a green circle.

location recorded within ±1 s (0.3%), producing RFID point clouds for individual tagged particles.

Once injected, particles were tracked from 15 August – 17 October 2021 with the roving antenna, on an almost daily basis until 10 September (26 surveys, Table S1). To conduct a survey, the operator walked across the non-debris-covered zone of the lower glacier snout with the roving antenna, following a 4 km long, predefined master track with 5–20 m between survey lines that ran transverse to the ice flow direction (Fig. 6b). A single line was also walked approximately along the subglacial channel centreline. Surveys required ~2 hours to cover an area of 0.1 km². The extent and position of the track was chosen to cover a broad zone above the 2018 subglacial channel position but was partially constrained by crevasses, ice collapse features, supraglacial meltwater channels, medial moraines and debris. The proglacial river was surveyed by walking along the channel banks and bars where possible. Surveys were performed in the hours around the river discharge minima when particle transport and radio signal attenuation was least likely. Due to weather and time constraints, 5 surveys in both the glacial and proglacial zones were incomplete, leaving a total of 16 complete surveys used for the assessment of the roving antenna system's overall particle localisation rate.

2.2.2. Planimetric particle localisation (2b)

The most likely planimetric location of individual tagged particles was determined by performing a probabilistic smoothing technique (density estimation) on the RFID point data using the following processing steps (see Fig. 2 for reference):

Step 2b-1 (Data subsetting):

The full roving antenna dataset containing all RFID data from all surveys was initially subset and grouped by unique combinations of particle ID and survey date to permit location estimation for individual particles on specific dates.

Step 2b-2 (Heuristic index):

A heuristic index was derived to account for the variable speed and track of the roving antenna, aiming to reduce bias caused by variation in the number of RFID points observed per unit area that may arise as a consequence. For each ID-survey date combination, the RFID points were first binned into a predefined 5-metre grid. The detection rate was then calculated for each grid square, based on the maximum possible number of observations given the total time spent surveying in the square and the tag transmission interval. Since signal strength provides a coarse indication of relative proximity to a tagged particle, mean RSSI was also calculated for each square and rescaled from 0 to 1 using the calibrated measurement range of the reader (200–110 RSSI). Values outside this range were rounded to the minimum or maximum calibrated value before rescaling. Accounting for both spatial and temporal variability in the speed and position of the roving antenna, alongside the information on relative proximity, a heuristic index for each grid square was defined as the product of mean rescaled RSSI and detection rate. Higher heuristic values are taken to represent a greater likelihood of a tagged particle being located in a given grid square.

Step 2b-3 (Kernel density estimation):

A weighted bivariate (2D) kernel density estimation (KDE) (Duong, 2007) was then applied to the binned RFID data, using the XY coordinates of the grid square centroids and a Gaussian kernel. The selection of this kernel is equivalent to assuming a normally distributed spatial uncertainty defined by a variable standard deviation (bandwidth). In the absence of reliable information on the detection range of the roving antenna across the survey area, the kernel bandwidth - essentially a smoothing parameter - was selected using Smoothed Cross-Validation (SCV) bandwidth optimisation (Duong and Hazelton, 2005; Chacón

and Duong, 2011). SCV optimises the bandwidth by iteratively minimising the Mean Integrated Squared Error (MISE) between the estimated density function and an unknown true density function, allowing for adaptive bandwidth selection that captures local data density variations and effectively balances over-smoothing and under-smoothing. SCV is able to capture the structure and complexity of both unimodal and multimodal data effectively while being fairly insensitive to outliers and noise. No correlation between the X and Y coordinate dimensions was observed in an exploratory data analysis, so a diagonal bandwidth matrix was used. A comparison of alternative bandwidth selectors is provided in the Supplementary Materials. The heuristic value was used as the KDE weighting parameter. KDEs were calculated for tagged particles with >= 3 received transmissions per survey and they were rescaled from 0 to 1 to allow intercomparison across surveys.

This analysis produced normalised 2D probability density estimates showing the likelihood that a tagged particle was located within a given grid square relative to the surveyed area. Any particles localised to the edge of an incomplete survey track were removed in this step. The spatial coverage (extent) of the survey was approximated using a 25 m buffer around the survey track for the purpose of illustration.

Step 2b-4 (Estimated planimetric location):

The centroid of the grid square with the highest probability density was taken as the estimated point location of the tagged particle at the median time of the survey. This is subsequently referred to as the KDE_{max} point. The contour encompassing 95% of the probability density estimate was taken as a confidence interval (CI) around each point. The assumption was made that smaller confidence interval (CI) contours were due to radio signal reception being primarily constrained to a small zone directly above the tagged particle, where the distance between the particle and the roving antenna was shortest but at the limit of detection range. When performed for each unique particle ID-survey date combination, this analysis revealed the change in the most likely planimetric position of tagged particles over the duration of the experiment.

The effective maximum horizontal detection range of the roving antenna was estimated using the 99th percentile of the distance between the RFID points (from all surveys) and their corresponding KDE_{max} points, assuming the KDE_{max} point locations were true.

The overall particle localisation rate of the roving antenna was assessed using the subset of particles that were ultimately detected by the proglacial antennas. This is calculated as the total number of successful daily particle localisations divided by the total number possible for the subset over the study duration. The subset was selected since these particles could be confirmed to reside within the survey area prior to their detection at the proglacial antennas.

2.2.3. Particle transport distance (2c)

Provided a reasonable spatial representation of the subglacial and proglacial channel centreline is available, the planimetric position of the KDE_{max} points may be translated into downstream transport distance. In this study, the proglacial channel segment was digitised using an orthoimage from August 2021. Since the subglacial channel had shifted from its 2018 position at the drilling transect and more recent GPR or surface-lowering measurements were not available, an alternative method was needed to determine its location in 2021. Data exploration revealed that the KDE_{max} points (n = 399) for all 56 particles in all surveys formed a linear cluster resembling the 2018 channel, which was interpreted as representing the channel's position in 2021. The subglacial channel centreline was therefore approximated as a lightly smoothed linestring running through the cluster (Fig. 9).

Each KDE was clipped to its 95% CI contour and then again to the grid squares intersecting the channel centreline. The probability density values of the clipped KDE were then mapped to the centreline using the closest point along the linestring to each grid square centroid. The along-channel distance from the injection borehole to the mapped probability density points was calculated and linearly interpolated to 1 m resolution. Along-channel probability density was also rescaled from 0 to 1 for comparison across daily surveys. The corresponding KDE_{max} point was subsequently mapped to the point along the channel centreline with the highest probability density value. The along-channel distance to this point was taken as the most likely particle transport distance. An estimate of uncertainty was obtained by calculating the along-channel distance to the upper and lower intersections of the 95% CI contour (Fig. 10).

When performed for all particle-survey combinations, this analysis produced a daily record of individual particle transport distance over time. A simple, continuous particle transport distance model was created for each particle using linear interpolation between the most likely transport distances.

2.3. Stationary antenna surveys (3)

2.3.1. Supraglacial antenna array

Fourteen stationary antennas (ELA Slender III) were placed in 2021 over the 2018 subglacial channel position to obtain a record of the downstream passage of tagged particles through each antenna's sensing field. Antennas were positioned horizontally on the glacier surface and grouped in pairs spaced 40–60 m apart for redundancy (Figs. 1; 7a). The distance between the antennas in each pair was 10–15 m. Each antenna was connected to an RFID reader with a 5–10 m coaxial cable. The readers were connected to individual RSlogger Basic Industrial dataloggers manufactured by Electroware, PL, which recorded and time-stamped the reader output over RS-232 connection. The internal datalogger clocks were synchronised to GNSS time ±5 s. The systems were powered with 12 V, 22 Ah batteries and 30 W solar panels. The data recording and power supply electronics were housed in insulated, waterproof boxes and the antenna housing was sealed to prevent water ingress.

To limit power consumption related to data storage, the RFID readers were programmed to record only the start and end times of periods in which a tagged particle was in range of an antenna. To achieve this, the reception of a transmission from a single tagged particle initiated or restarted a 20 s countdown during which the particle was assumed to be in range. If no further transmissions from the particle were recorded during the countdown, the in-range period ended. The number of seconds a tagged particle was in range of each antenna per 1-hour timestep was then calculated. A 'time-in-range per timestep' threshold was applied to timeseries affected by low amounts of noise in the form of highly implausible, very short-duration detections. These were likely caused by the false validation of radio signals from particles with similar ID codes that were corrupted by heavy attenuation and scattering, and by limitations in the reader's checksum validation protocol. The continual functioning of each antenna was assessed using dedicated RFID tags placed on each power supply box and emitting at 15 s intervals, assuming that gaps in the test tag's 'in-range' record indicate equipment malfunction.

A maximum estimate of the coverage of each antenna's sensing field along the subglacial channel was derived using a circular buffer around each antenna, with a diameter corresponding to the estimated maximum horizontal range of the roving antenna. The along-channel distance to the intersections of each antenna's buffer with the channel centreline defined the transport distance
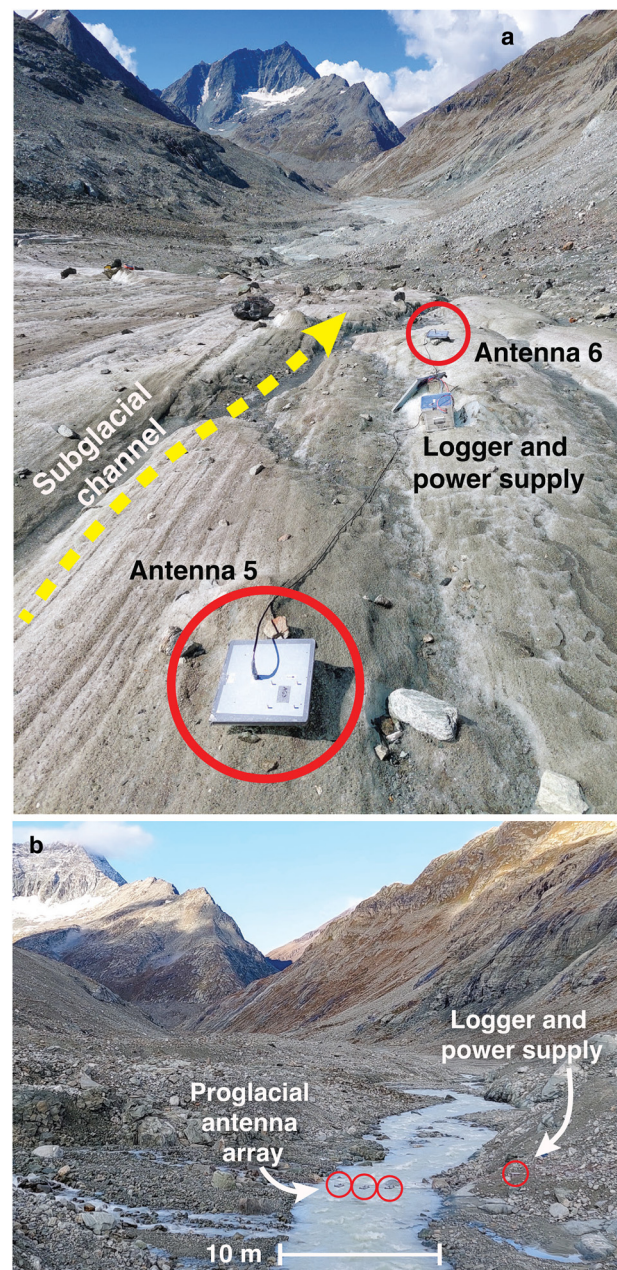

Figure 7. Supraglacial and proglacial antenna systems. a) Supraglacial antenna pair (5 and 6) positioned approximately over the subglacial channel (yellow line) ~35 m below. (b) The proglacial antenna array located 140 m downstream of the subglacial channel outlet.

uncertainty range for an individual received transmission at the antenna.

2.3.2. Proglacial antenna array

Three stationary antennas (ELA Slender III) were suspended 1.5 m apart across a 12 m wide, bedrock-confined cross-section of the proglacial river at a height of 1.4 m above the riverbed, located 140 m downstream of the subglacial channel outlet (Figs. 1; 7b). The array was used to detect the passage of tagged particles past a fixed proglacial location, confirming their emergence from the glacier and recording tags that would otherwise be missed due to detection range or survey timing limitations with the roving antenna and the supraglacial array. The antennas were sealed to prevent water ingress and angled downstream, ~12° off horizontal, limiting the upstream coverage of the antenna sensing fields to avoid early particle detection. Each antenna was

connected with a 10 m coaxial cable to an individual RFID reader and an RSlogger datalogger located on the northern riverbank and programmed identically to the supraglacial antennas.

Field tests were performed to assess the detection rate of the array for particles emitting at 200, 600 and 1200 ms time intervals, at high river stage (0.89 m) and discharge (10.2 m^3 s^{-1}), as well as low stage (0.55 m) and discharge (4.5 m^3 s^{-1}). River gauging was performed at a site 100 m downstream of the antennas (Müller and Miesen, 2022). For each interval, a tagged particle was attached to the end of a rope, thrown ten times into the river ~30 m upstream of the antennas, then allowed to travel underneath them along the river thalweg. The number of throws in which the array as a single unit detected each particle was counted to determine the detection rate.

The detection rate for freely travelling tagged particles was also assessed by injecting particles emitting at 200 ms time intervals 80 m upstream of the array at high (9.1 m^3 s^{-1}, $n = 17$) and low (2.8 m^3 s^{-1}, $n = 15$) discharge, then calculating the percentage of particles that were ultimately detected by the proglacial array over the following days. Particles were proclaimed missing if they were not detected by the proglacial array and could not be localised later with the roving antenna at low discharge. The detection rate at the proglacial antennas was assessed by accounting for all potential particle passes, including all roped particle throws (200 ms interval) and freely injected test particles.

A tagged particle on a rope was used to determine the maximum upstream detection distance of the proglacial antennas at low stage (0.56 m) and discharge (3.2 m^3 s^{-1}). The particle was allowed to travel slowly downstream along the river thalweg at 1 m intervals from a point 30 m upstream, and the location at which the particle was first detected was noted.

2.4. Particle transport distance model (4)

The linear transport distance model produced for each tagged particle by the roving antenna analysis was manually adjusted to account for the information on the timing of particle motion provided by the stationary antennas. Adjustment was performed by adding points that forced each model to pass through the hourly 'in-range' markers, provided the two independent records were in overall coherence. Step-wise adjustments were preferenced in periods where the stationary antenna data were abundant, broadly reflecting the periods of extended rest and the more rapid transport steps that bedload theoretically undergoes (e.g. Einstein, 1937; Hassan and others, 2013). In cases where two in-range markers overlapped, the particle was assumed to reside within the overlapping zone. The most probable roving antenna transport distances were taken as fixed, except in cases where short transport distance reversals were eliminated. The probability density values within the 95% confidence interval provided context for this process of refinement, which is largely subjective since the estimated range of the supraglacial antennas is broad and particles may not be detected consistently.

3. Results

3.1. Roving antenna surveys

To illustrate the analysis used to determine the planimetric location of a tagged particle, the results of the processing steps (phases 2b, 2c) are presented for a single tagged particle (P1) in Figs. 8, 9 and 10 (data from all particles used in Fig. 9). The spatial distribution of the RFID points obtained during the survey on 20 August was typical of particles detected in the mid to lower region of the glacial survey area, where the roving antenna track was not constrained by ice collapse features and ice was thin (<30 m). Although partially affected by artefacts related to the coarse survey lines, the RFID point cloud was dense ($n = 690$) and radially distributed, with RSSI values and number of observations generally increasing towards a focal region close to the estimated channel centreline (Fig. 8a). The heuristic index calculated for each grid square using these RFID points was similarly concentrated (Fig. 8b), along with the resulting weighted KDE (Fig. 8c). The change in the planimetric position of the tagged particle over time was revealed by applying the analysis over multiple daily surveys, showing a progressive downstream transport with rest periods of up to two days (Fig. 8d). The relationship between the KDEs, their 95% CIs, KDE$_{max}$ points and the most likely along-channel transport distances is illustrated for particle P1 on 18 August (Fig. 10).

In general, the KDE$_{max}$ point locations were insensitive to large changes in kernel bandwidth, differing by 1–2 adjacent grid squares ($\pm 5-10$ m) across bandwidth selectors and fixed bandwidth values (Supplementary Materials). The use of the heuristic index as a KDE weighting parameter was effective at reducing bias caused by variability in survey line position and speed, and at accounting for information on particle proximity provided by the RSSI measurements (Supplementary Materials).

Each of the particles presented in detail (P1-4) was successfully localised on each day that it was situated in the glacial and proglacial survey zones, except for P1 and P2 on 23 August due to an incomplete survey in the crevassed region of the lower glacier snout. These particles were transported through the subglacial channel within 4–8 days of injection (Fig. 11). Of the entire batch of 56 injected particles, no data was obtained for three particles (5.4%). Accounting for all potential daily point localisations for the particles that were eventually observed at the proglacial antennas, the overall localisation rate was 75%. Particles were localised to a maximum ice depth of 47 m with a minimum of three and a maximum of 2059 RFID points.

Particles were consistently localised over consecutive days to the same or adjacent grid squares ($\pm 5-10$ m) and to within 5–10 m difference of transport distance (e.g. 18–20 August in Fig. 11b) in the mid-upper to lower survey area (100–500 m transport distance). This consistency was observed despite spatial and temporal variation in the detection rate and strength of received transmissions. In the upper 100 m of the survey, KDE$_{max}$ points were more dispersed and particles were generally localised to within 25 m of transport distance (<5 grid squares) across consecutive surveys (Fig. 9); related to sparser RFID point clouds and greater ice depth (42–47 m). The mean range of all 95% transport distance uncertainty estimates was 49.8 m (9.4% of the overall channel centreline length).

The estimated maximum horizontal range of the roving antenna in both the subglacial and proglacial zones is 38 m, based on the 99th percentile of the distance between all RFID points ($n = 91, 437$) and their corresponding KDE$_{max}$ points, for all particle ID-survey date combinations ($n = 399$).

Particle P2 was identified visually on the true-right bank of the proglacial river during a roving antenna survey. The particle was localised to the correct 5 m grid square in the roving antenna analysis and it sustained no damage over the 500 m transport distance.

3.2. Supraglacial stationary antenna surveys

Based on the estimated horizontal detection range of each antenna (38 m), the length of the subglacial channel was covered by two or more antennas (Fig. 12). In general, the particles were detected consistently along the subglacial channel,
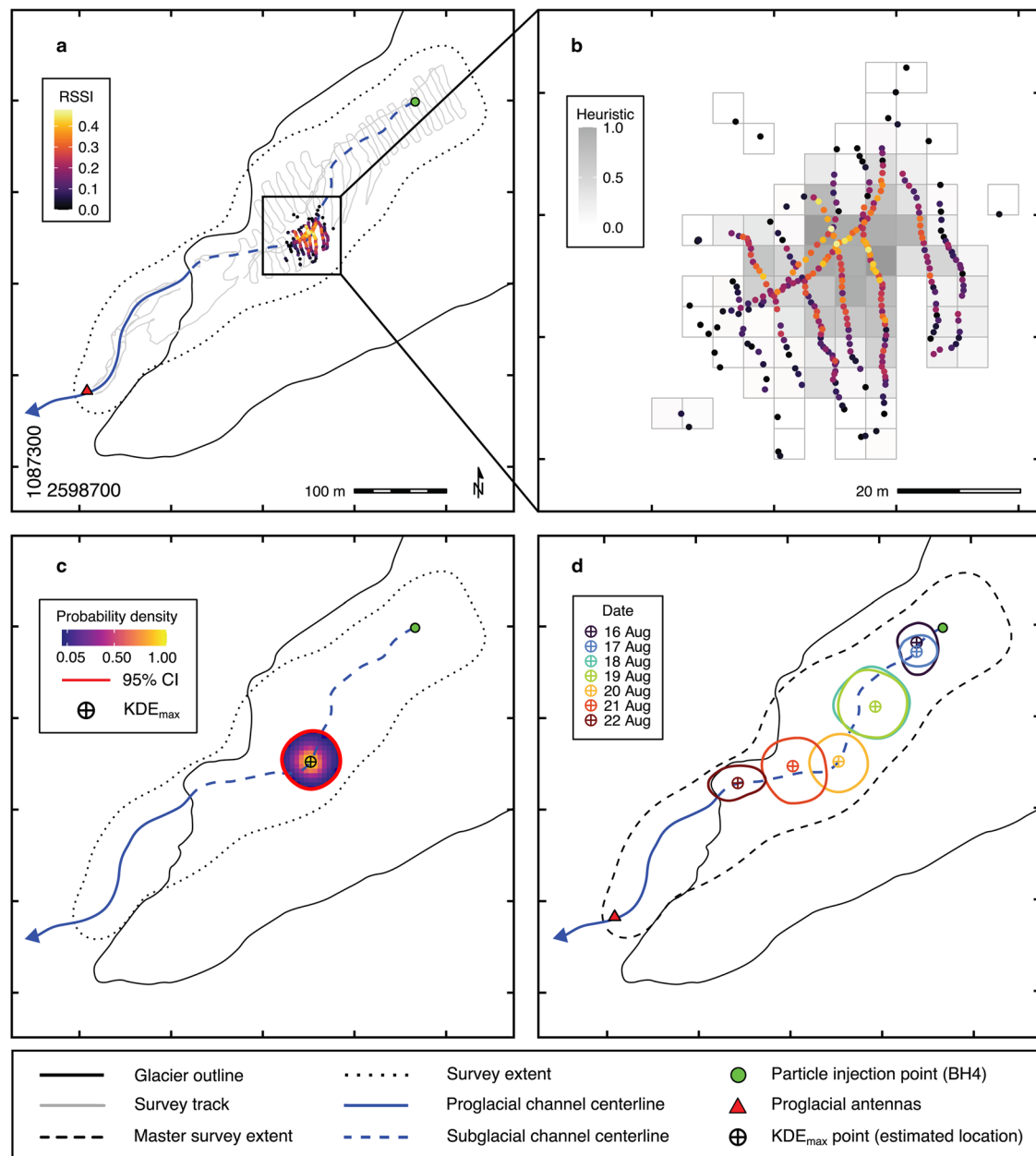
Figure 8. Tagged particle localisation using a roving antenna. (a) Spatial distribution and rescaled signal strength (RSSI) of received radio transmissions from a single tagged particle (P1) observed during a roving antenna survey on 20 August 2021 ($n = 690$). (b) Close-up of the gridded heuristic index data derived from the binned RFID points in panel a, accounting for detection rate and mean RSSI per 5 m grid square. (c) Weighted 2D KDE performed on the heuristic index data in panel b, and the resulting estimated point location of the tagged particle (KDE$_{max}$) with 95% CI contour. (d) Change in KDE$_{max}$ position with corresponding 95% CI contours over consecutive daily surveys.

though there were some extended periods in which they were detected intermittently or not at all (e.g. P3 from 15–18 August in Fig. 11). The test tag detection record indicated that the antennas were continuously active. Particles were observed through up to ~47 m of temperate glacier ice and 0.9 m of turbid meltwater by the two uppermost stationary antennas, indicating that the maximum working depth of the RFID equipment was not exceeded, although this is likely close to the limit.

There was strong coherence between the independent roving and stationary antenna transport distance records, with the stationary antenna data supporting the daily transport distances produced by the roving antenna analyses and revealing the sub-daily periods during which particles were transported downstream between antenna pairs (e.g. P3 on 18 August in Fig. 11c). Fig. 11 shows the non-adjusted and manually adjusted transport

distance models utilising both the roving antenna and stationary antenna data for all four particles injected into the subglacial channel. The manually adjusted transport distance models for particles P1–4 are plotted together in Fig. 13, revealing the differences in the timing of particle movement through the subglacial and proglacial channels. Although the transport duration in the subglacial channel reach was similar for P1–4, the particles were not transported together and underwent fewer periods of rest in the proglacial channel.

3.3. Proglacial stationary antennas

100% of the tagged particles attached to a rope were detected by the proglacial antennas at high stage (0.89 m) and discharge (10.2 m^3 s^{-1}), except for the particle transmitting at a 2200 ms interval, for which only 20% of the passes under the antennas were
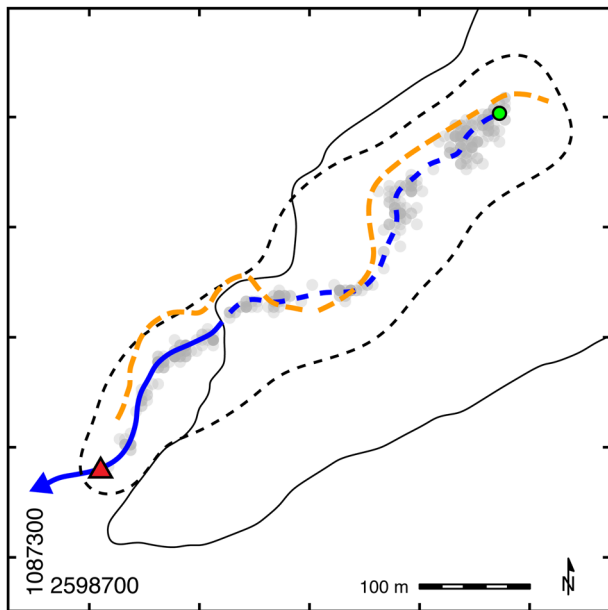
Figure 9. The estimated location of the subglacial channel in 2021 (dashed blue line). Derived by linking linear clusters of all KDE$_{max}$ points (grey points) produced for the 56 particles in all roving antenna surveys ($n = 399$). The 2018 subglacial channel centreline (dashed orange line) is shown for reference (adapted from Egli and others, 2021a). See Fig. 8 for main legend.

observed (Table 1). However, 100% of the 2200 ms tagged particle throws were detected at low stage (0.55 m) and discharge (4.5 m^3 s^{-1}). The river discharge was greater than the high discharge at the time of testing for 2.8% of the 2021 record (max: 13.2 m^3 s^{-1}), and was less than the low discharge for 28.7% of the 2021 record (min: 1.4 m^3 s^{-1}).

Of the 32 tagged particles injected freely in the proglacial river, 31 (98.7%) were detected by the proglacial antennas over the course of 3.5 days and 24 (75%) were detected within 3 hours of injection. The single tagged particle that was not detected could not be located with the roving antenna either, so was

assumed to have been missed by the proglacial antennas. 28 tagged particles, including P1, P3 and P4, were detected by the proglacial antennas, having travelled through 500 m of subglacial and proglacial channel (Fig. 11).

Accounting for the roped particle throws (200 ms interval) and the freely injected test particles, there were a total of 52 potential tagged particle passes under the proglacial antennas across low to high stage (0.45–0.89 m) and discharge (2.3–10.2 m^3 s^{-1}) conditions. A single particle went undetected, producing an overall detection rate of 98.1% at the proglacial antennas. The maximum distance that a tagged particle could be detected upstream of the proglacial antennas was 14 m. The test tag detection record indicated that the antennas were continuously active.

4. Discussion

Our results demonstrate the ability of both the independent roving antenna and the stationary antenna systems to track a-UHF RFID-tagged particles through snout-marginal subglacial and proglacial survey areas of Alpine glaciers. Although each system has the potential to be used in isolation for bulk particle tracking studies in both environments, combining the spatially rich Lagrangian roving antenna data and the temporally rich Eulerian stationary antenna data was effective; capturing both daily planimetric position and transport distance alongside the sub-daily timing of particle motion. When combined with continuous water and sediment discharge data from proglacial marginal zones, this information may be used to quantify and describe subglacial sediment transport and the driving mechanisms in a holistic Lagrangian–Eulerian analytical framework (e.g. Ballio and others, 2018). This is likely to be particularly effective where a large number of particles of a broad range of grain sizes, shapes and densities are used.

4.1. Roving antenna surveys

The roving antenna produced a record of planimetric particle position (KDE$_{max}$ points) during a given survey, which served
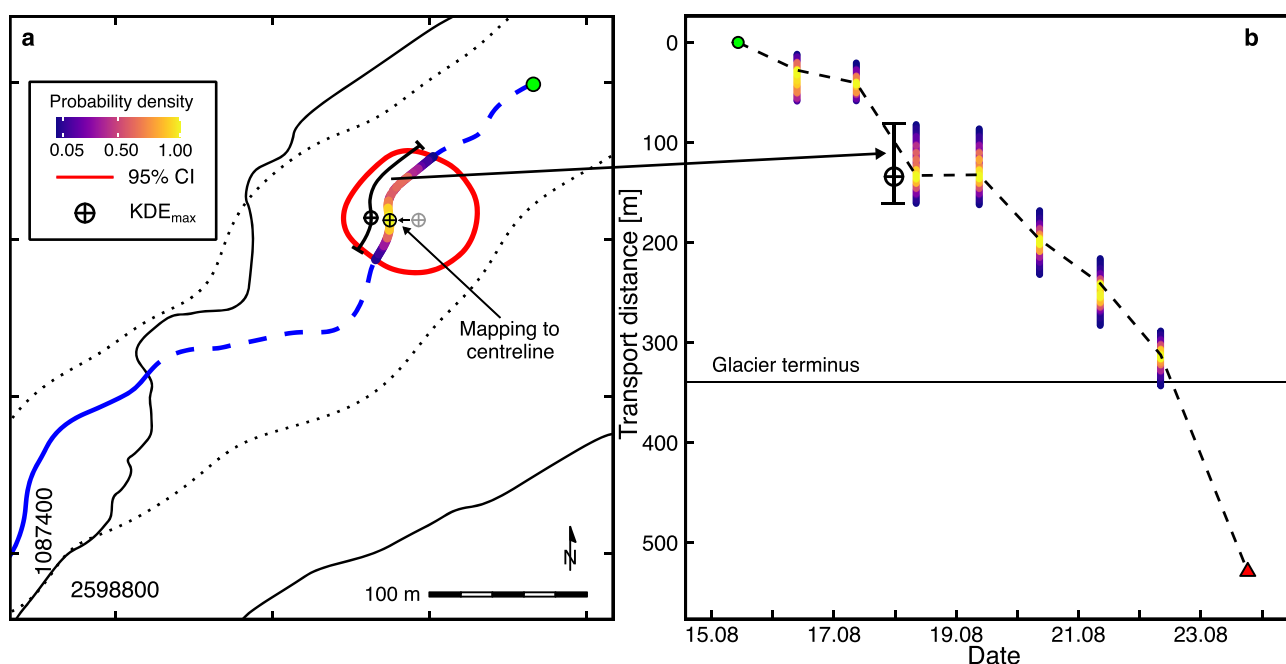

Figure 10. Translating planimetric particle location to downstream transport distance from the injection borehole. (a) Deriving along-channel transport distance for particle P1 on 18 August 2021 by mapping the kernel density estimate to the estimated channel centreline. See Fig. 8 for main legend. (b) Roving antenna-based daily particle transport distances and a non-adjusted linear transport model (dashed black line) for particle P1.
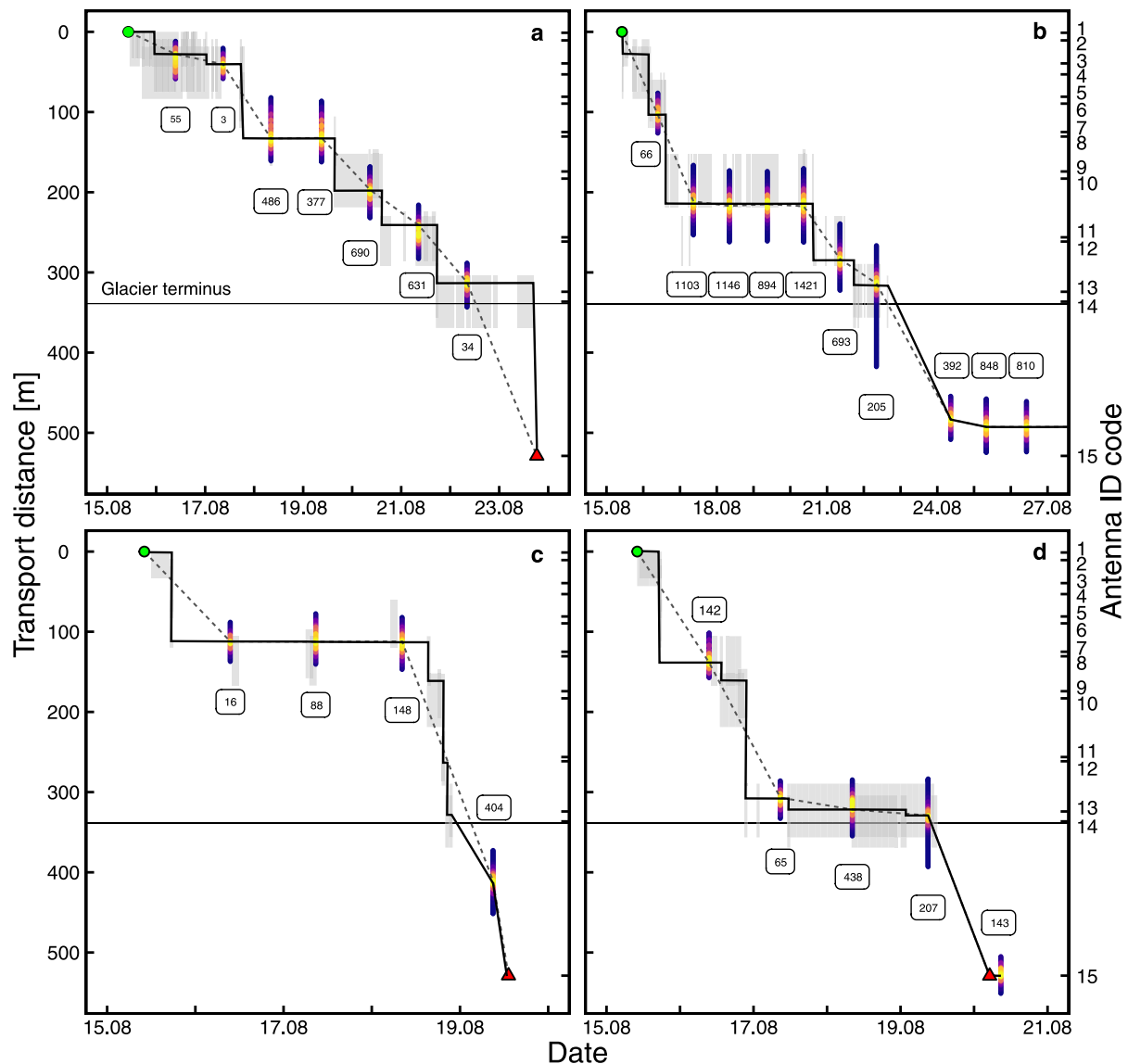
Figure 11. Adjusted (solid black line) and non-adjusted (dashed grey line) transport distance models for tagged particles P1–4 (panels a–d). Particle injection in the borehole and initial detection at the proglacial antennas indicated with a green point and a red triangle, respectively. Text boxes display the number of RFID points used to derive the roving antenna distance estimate. Vertical grey bars indicate the time periods in which the particle was in range of a stationary antenna. A stationary antenna noise threshold of 32, 80, 32 and 21 s h^{-1} was set for particles P1–4, respectively. The x-axes have different scales.

as the foundation for the particle transport distance models. The dependable localisation of particles and the positional consistency across consecutive days in the mid-upper to lower survey zone suggest that the probabilistic point localisation technique was relatively stable across space and time in this area despite variation in the RFID point clouds. This variation was caused by unknowable changes in radio signal attenuation and scattering, as well as antenna positioning, which will be specific to the survey area, scan lines and equipment used in each study. In the absence of validation data, which would require placing and monitoring multiple fixed particles along the subglacial channel (beyond the scope of this study), the spatial precision of the roving antenna analysis is estimated to be the same as the positional variability in the KDE$_{max}$ points over consecutive days in which the tagged particles were probably motionless: ±5−10 m in the mid-upper to lower survey zone, and ±5−15 m in the upper 100 m, depending on the quality of the RFID point cloud. Reduced precision in the upper zone is likely related to the thicker ice (~40−47 m) causing greater signal attenuation and scattering, resulting in sparser RFID point clouds. The 75% overall localisation rate is comparable

to those of fluvial particle tracking studies (Lamarre and others, 2005; Bradley and Tucker, 2012; Cassel and others, 2017), and was achieved with much greater distances between the RFID tags and the roving antenna through temperate ice and turbid meltwater. The total lack of data from 3 out of 56 particles (5.4%) may be related to their burial out of range or immediate failure of the RFID tag.

The records of change in tagged particle position over time (e.g. Fig. 8d) may be used to investigate the spatial dispersion of particles across subglacial or fluvial systems (e.g. Bradley and Tucker, 2012), provided the dispersion distances are larger than the precision of the point localisation, ideally by an order of magnitude. We show that large datasets of point location estimates can be used to map the reach-scale planform geometry of major subglacial channels (Fig. 9). This is primarily useful for mapping the most probable flow path of the tagged particles for transport distance estimation in the absence of geophysical measurements, but intensive studies performed over multiple years may also reveal changes in channel position and lead to insights into the impact of subglacial channel position and morphology on sediment transport and export.
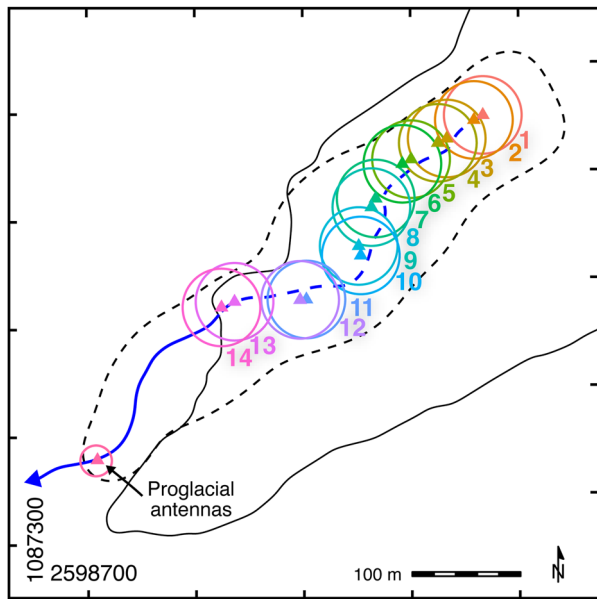
Figure 12. The estimated planimetric coverage of each stationary antenna's (triangle) sensing field (circle) along the estimated subglacial channel centreline. See Fig. 8 for main legend.

Table 1. Detection rate of roped tagged particles transmitting with different time intervals at the proglacial antenna array, for both high and low river stage and discharge (Q_w)

	Transmission interval [ms]		
	200	600	2200
High Q_w (10.2 m³ s⁻¹)	100%	100%	20%
Low Q_w (4.5 m³ s⁻¹)	100%	NA	100%

No data was collected for the 600 ms interval at low discharge because the rope was destroyed by the river.

(2012); Hassan and others (2013); Ballio and others (2018) and Lane and Nienow (2019). The overall number of particles required will depend on the process of interest, the characteristics of the study site, the particle detection rate and the statistical power and precision desired. We suggest a minimum of 200–300 particles for studies at the same spatial scale as this one. The few transport distance results presented here as a proof-of-concept for the method are in accordance with recent field and modelling-based studies which suggest that subglacial sediment transport may be attenuated in non-pressurised subglacial channels under rapidly thinning and retreating glacier ice on the order of days to weeks or longer (Beaud and others, 2018; Perolo and others, 2019).

The probabilistic localisation method presented here is flexible due to the data-adaptive smoothing parameter (kernel bandwidth). This allows for a relatively coarse survey line spacing (e.g. 20 m) and sparse RFID point clouds across a range of lossy signal propagation media (ice, water, rock, air). In addition, it does not require prior work with reference particles or the use of complex signal propagation models (*cf.* Li and others, 2019; Cassel and others, 2021). The approach to field data collection and analysis is therefore optimised for rapidity and functional application at scale, at the potential expense of very high localisation precision. It is important to note that the point localisation and uncertainty estimations are probabilistic in nature, grounded in the assumption that the RFID point clouds and the resulting density estimates are focussed on the true point location of an RFID-tagged particle. However, this would not hold in cases where transmissions are severely attenuated or reflected directly above the particle and would hold to a lesser extent in cases where the particles are further away from the antenna, leading to positional error. The use of a bandwidth selector that minimises under-smoothing is therefore recommended to account for this potentiality when estimating positional uncertainty. An exploratory analysis of the effect of the KDE free parameters on particle localisation is recommended on a per-study basis, giving primary consideration to the compromise between estimated localisation precision and uncertainty, and bias towards the survey lines. It may be reasonable to use a lower confidence interval (e.g. 50%), smaller grid sizes, lower bandwidth values or a signal strength threshold to produce smaller uncertainty intervals or more precise KDE_{max} points in cases where the RFID data are known to be robust (*i.e.* abundant, highly focussed and derived from dense survey lines).

To achieve robust RFID data and point location estimates, the survey should be performed in the hours around the discharge minima, the track should completely cover the channel reach of interest and the line spacing should ensure a wide overlap in the coverage of the antenna sensing field along the channel. Dense line spacing is likely to produce more accurate positional estimates at the cost of significantly increased field efforts. Although not tested, the reduced precision in the upper 100 m of the survey area indicates that the ice depth was close to the limit in this study. Surveying more slowly and making repeat

The tagged particle point locations were converted into a record of downstream transport distance by mapping them onto the estimated 2021 subglacial channel centreline. The non-adjusted linear transport distance models generated from this data may be used (when large numbers of particles are tracked) to analyse coarse sediment mobility at sub-seasonal to multi-annual timescales and permit temporally averaged, statistical generalisations about particle residence times, cumulative displacements, rest times and displacement rates both over the entire survey zone and within specific channel reaches. Where water discharge data are available, daily particle transport distance may be related to, for example, flow regime (particularly in terms of diurnal discharge amplitudes), Shannon entropy, critical discharge and sediment entrainment thresholds, following analytical methods outlined in Hassan and others (1992); Bradley and Tucker
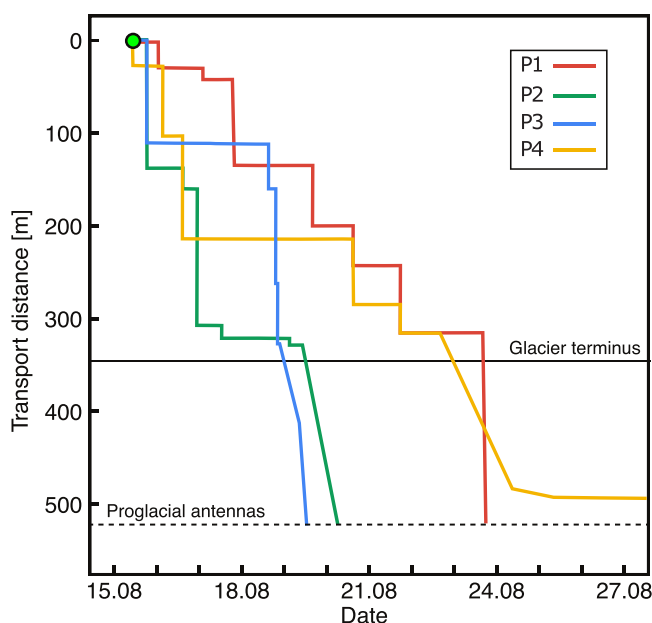

Figure 13. The adjusted transport distance models for subglacially deployed tagged particles P1–4.

passes in zones of deeper ice (e.g. 40–50 m) may improve the localisation precision. If the location of the subglacial channel is known in advance, it may be possible to use a relatively short, efficient survey track focussed directly over the channel, enabling larger along-channel distances to be covered or repeat sub-daily surveys of a smaller area. A drone-based roving antenna (e.g. Cassel and others, 2020) capable of low-level flight along survey lines may enable precise, dense, potentially rapid surveys of large areas with reduced physical effort and allow impassable areas to be surveyed. Alternatively, an autonomous snowmobile or vehicle presents another viable solution, facilitating surveys at slower speeds and with better ground coupling to improve signal reception. The vehicle may also be used to perform GPR surveys at the same time. The up to 1 s delay in RFID transmission-reception and dGNSS logging also introduces a degree of error, potentially causing RFID signals to be incorrectly assigned to the adjacent grid square, though the overall impact on particle localisation is likely to be low where tens to hundreds of transmissions are received.

The reliability of the transport distance results also depends on the accuracy of the channel centreline feature used, highlighting the importance of establishing the channel position as comprehensively as possible prior to or during a survey campaign. The use of all planimetric particle locations to estimate the 2021 channel position is unvalidated and therefore represents a source of uncertainty and potential error in transport distance estimates. This method may be adapted to use multi-threaded linestrings or polygonal spatial features describing braided or broad channel systems. The positional variance around the estimated centreline in this study is likely a consequence of actual spatial dispersion around the centreline as well as artefacts caused by the precision and gridded nature of the density estimates. Even in cases where the channel position is not precisely known, an informed approximation of its centreline may still provide valuable information on particle transport distances.

4.2. Supraglacial stationary antenna surveys

The stationary supraglacial antenna array was used to complement the roving antenna analyses, providing information on the sub-daily timing and distance of tagged particle transport at an hourly resolution and allowing for refinement of the linear transport distance models. The intermittency in particle detection at individual antennas is likely related to particles passing in and out of range due to changes in tag and antenna positioning, as well as to environmental changes affecting signal propagation. In comparison to the roving antenna, the stationary antenna array was autonomous and required significantly less in-field effort for data collection. In our experiment, weekly maintenance was required once installed as ice surface melt caused the antennas to shift position over time. Development of a gimballed fixation system may facilitate greater operational autonomy. The antenna detection range may be improved by eliminating the use of coaxial cables which result in a signal path loss of ∼0.3 dB per metre. To achieve this, stationary antennas with individual reader and power supply systems mounted directly to each antenna may be constructed.

The array was, however, spatially limited since particles could only be localised to within a relatively broad zone (38 m radius) and particle motion within that zone was not discernible. Nevertheless, in cases where two or more hourly in-range markers overlapped, the particle was highly likely to have resided within the overlapping zone (e.g. P4 on 16 August), providing a more accurate transport distance estimate at that time. The use of a dense array with multiple overlapping antenna sensing fields is therefore strongly recommended, though further testing is

required to be able to evaluate the optimal number and pattern of antennas for a given study site in advance. Although the placement of fixed reference particles along the subglacial channel may help constrain antenna detection ranges, the fieldwork required to install them would be prohibitive in most cases.

Given the benefits of overlapping antenna sensing fields and the relative consistency of tagged particle detection, particularly during periods in which they moved (potentially a consequence of the rapidly changing orientation of the tag and greater variability in signal propagation paths), it may be feasible to use an array of stationary antennas as a standalone method for particle tracking, with significantly reduced fieldwork requirements. This may be best achieved using a dense, 2D array of supraglacial antennas with overlapping sensing fields (e.g. a grid of antennas placed at 10 m intervals over the channel), with each antenna programmed to record all received transmissions and their strength. The spatial relationship between the rate and strength of detections across the grid may then be analysed statistically to determine the zone in which the tagged particle is most likely to reside at a given time.

4.3. Proglacial antenna array

The proglacial antennas were used to observe tagged particles after their emergence from the glacier, acting as a 'gate' marking the time the particle left the master survey area. The high particle detection rates observed during testing are comparable to those reported for passive RFID-tagged particles (Lamarre and others, 2005; Bradley and Tucker, 2012; Hassan and Roy, 2016) but were achieved in a large, highly turbulent proglacial river system. A single proglacial antenna array may be used as a standalone method of subglacial particle tracking if it is placed adjacent to the subglacial channel portal, providing data on the overall transport duration and displacement velocity of coarse a-UHF RFID-tagged sediment through a single reach of subglacial channel. Multiple arrays of this kind spaced along a proglacial river can provide robust information on reach-scale transport durations and displacement velocities. The tests performed at the proglacial antennas show that radio tag transmission interval strongly affects the likelihood of particle detection at high stage and discharge. Detection rate and range tests should therefore be made on a per-site basis to determine the minimum transmission interval that provides reliable detection rates across the range of stage and discharge conditions. Where the maximum operational water and / or ice depths are approached, a faster transmission interval should be used to maximise the chance of transmissions being received.

4.4. Additional suggestions for development

Although the changes in particle density caused by tagging were low, the potential impact of tagging on particle transport may be reduced by removing the low-density plastic housing from the COIN ID tag (Ø24 × 6.5 mm, 5 g). The tag may then be carefully waterproofed with epoxy before insertion into a particle. Housing removal would also facilitate the insertion of additional batteries to extend operational life, or the tagging of particles with b-axes <40 mm. Where antenna detection ranges and rates are known to be sufficient, decreasing the tag transmission interval would also increase operational life and enable particle tracking studies running over multiple years. This would allow the deployment of tagged particles a substantial distance away from the main subglacial channel to assess coarse sediment mobility across the glacier bed over multi-annual timescales.

The miniaturisation of wireless sensor platforms or 'smart' particles that provide information on the particle's environment and/or motion (e.g. Bagshaw and others, 2012, 2014; Olinde and Johnson, 2015; Hart and others, 2019; Prior-Jones and others, 2021) would

prove invaluable to large-scale subglacial particle tracking studies in heterogeneous glacier ice, affording greater insight into the processes driving subglacial sediment transport when combined with hydrological information. We envisage the development of open-source, biodegradable transmitters, sensor platforms and tagged particles that can be rapidly reproduced using low-cost 3D printing or moulding technologies and commercially available electronic components. The cost of each single-antenna system used in this study is approximately 900–1000 EUR at the time of publication (see also Cassel and others, 2021). Additionally, each tagged particle costs around 17–20 EUR to produce. Developing affordable, open-source a-UHF RFID hardware could facilitate the wider use of active particle tracking in various environments, enabling the collection of the large volumes of data needed to elucidate the processes driving coarse sediment transport.

The development of small active RFID transmitters operating at longer wavelengths (e.g. VHF) with a high transmit power might facilitate the detection of tagged particles through deeper temperate ice and potentially at greater submergence depths in subglacial channels. Applications of this method higher up-glacier may provide invaluable field-based insights into unresolved scientific questions on how subglacially eroded sediment is transported in pressurised versus non-pressurised channels, through channelised versus distributed drainage networks and on how sediment is transported into subglacial channels, and eventually into subglacial landforms and the proglacial sedimentary record. Although not tested, the planimetric localisation precisions and increase in RSSI with proximity to a tagged particle indicate that particles may be recovered from proglacial floodplains at low-flow conditions using a fine grid search with a roving antenna. This may enable the assessment of particle rounding and fining in subglacial channels or the downloading of data from environmental sensors embedded in smart particles.

5. Conclusions

This study successfully demonstrated the use of a-UHF RFID transmitters for tracking coarse sediment particles as they are transported through large meltwater channels underneath shallow temperate ice, as well as through large, turbid proglacial rivers. The combined use of a spatially precise roving antenna system and a stationary antenna array with a high temporal resolution was effective at monitoring the change in position and timing of motion of tagged particles. Both the roving and stationary antenna systems were capable of particle detection rates that are comparable to those obtained in studies performed in rivers (>75%). The method may be used to obtain information on reach-scale particle transport durations, cumulative displacement, displacement rates, timing of motion and dispersion. When combined with river gauging, glaciological and meteorological data, process-based drivers of coarse subglacial sediment transport by meltwater may be revealed. This study therefore stands as a proof-of-concept for particle tracking-based investigations into coarse subglacial sediment transport mechanisms and process timescales on larger spatial scales and with greater particle sample sizes. The few transport distance results presented here support recent research suggesting that subglacial sediment transport in meltwater channels may be attenuated close to the terminus of rapidly retreating and thinning Alpine glaciers on the order days to weeks or longer. Future work will involve an in-depth analysis of several hundred tagged particles to investigate coarse sediment transport dynamics under the Glacier d'Otemma, Switzerland.

Supplementary Material. The supplementary material for this article can be found at https://doi.org/10.1017/jog.2023.77

References

Alexander A and 5 others (2020) Pressure and inertia sensing drifters for glacial hydrology flow path measurements. *The Cryosphere* **14**(3), 1009–1023. doi:10.5194/tc-14-1009-2020

Alley R and 5 others (1997) How glaciers entrain and transport basal sediment: physical constraints. *Quaternary Science Reviews* **16**(9), 1017–1038. doi:10.1016/S0277-3791(97)00034-6

Alley R, Cuffey K and Zoet L (2019) Glacial erosion: status and outlook. *Annals of Glaciology* **60**(80), 1–13. doi:10.1017/aog.2019.38

Bagshaw E and 6 others (2014) Novel wireless sensors for in situ measurement of sub-ice hydrologic systems. *Annals of Glaciology* **55**(65), 41–50. doi:10.3189/2014AoG65A007

Bagshaw EA and 7 others (2012) E-tracers: Development of a low cost wireless technique for exploring sub-surface hydrological systems. *Hydrological Processes* **26**(20), 3157–3160. doi:10.1002/hyp.9451

Ballio F, Pokrajac D, Radice A and Hosseini Sadabadi SA (2018) Lagrangian and Eulerian description of bed load transport. *Journal of Geophysical Research: Earth Surface* **123**(2), 384–408. doi:10.1002/2016JF004087

Barwick S, Besson D, Gorham P and Saltzberg D (2005) South Polar in situ radio-frequency ice attenuation. *Journal of Glaciology* **51**(173), 231–238. doi:10.3189/172756505781829467

Beaud F, Flowers GE and Venditti JG (2018a) Modeling sediment transport in ice-walled subglacial channels and its implications for esker formation and proglacial sediment yields. *Journal of Geophysical Research: Earth Surface* **123**(12), 3206–3227. doi:10.1029/2018JF004779

Beaud F, Venditti JG, Flowers GE and Koppes M (2018b) Excavation of subglacial bedrock channels by seasonal meltwater flow. *Earth Surface Processes and Landforms* **43**(9), 1960–1972. doi:10.1002/esp.4367

Bradley N and Tucker GE (2012) Measuring gravel transport and dispersion in a mountain river using passive radio tracers. *Earth Surface Processes and Landforms* **37**(10), 1034–1045. doi:10.1002/esp.3223

Burri M, dal Piaz GV, della Valle G, Gouffon Y and Guermani A (1999) Chanrion (CN 1346) avec partie nord de la feuille Mont Vélan (CN 1366). Topographie: Carte nationale de la Suisse 1:25000. In *Atlas Géologique de La Suisse*, Carte 101. Bern, Switzerland: Service hydrologique et géologique national.

Cassel M, Dépret T and Piégay H (2017) Assessment of a new solution for tracking pebbles in rivers based on active RFID. *Earth Surface Processes and Landforms* **42**(13), 1938–1951. doi:10.1002/esp.4152

Cassel M and 6 others (2020) Comparison of ground-based and UAV a-UHF artificial tracer mobility monitoring methods on a braided river. *Earth Surface Processes and Landforms* **45**(5), 1123–1140. doi:10.1002/esp.4777

Cassel M, Navratil O, Perret F and Piégay H (2021) The e-RFIDuino: An Arduino-based RFID environmental station to monitor mobile tags. *HardwareX* **10**, e00210. doi:10.1016/j.ohx.2021.e00210

Chacón JE and Duong T (2011) Unconstrained pilot selectors for smoothed cross-validation. *Australian & New Zealand Journal of Statistics* **53**(3), 331–351. doi:10.1111/j.1467-842X.2011.00639.x

Cook SJ, Swift DA, Kirkbride MP, Knight PG and Waller RI (2020) The empirical basis for modelling glacial erosion rates. *Nature Communications* **11**(1), 759. doi:10.1038/s41467-020-14583-8

Delaney I and Adhikari S (2020) Increased subglacial sediment discharge in a warming climate: consideration of ice dynamics, glacial erosion, and fluvial sediment transport. *Geophysical Research Letters* **47**(7), e2019GL085672. doi:10.1029/2019GL085672)

Duong T (2007) Ks: kernel density estimation and kernel discriminant analysis for multivariate data in R. *Journal of Statistical Software* **21**, 1–16. doi:10.18637/jss.v021.i07

Duong T and Hazelton ML (2005) Cross-validation bandwidth matrices for multivariate Kernel density estimation. *Scandinavian Journal of Statistics* **32**(3), 485–506. doi:10.1111/j.1467-9469.2005.00445.x

Egli PE, Belotti B, Ouvry B, Irving J and Lane SN (2021a) Subglacial channels, climate warming, and increasing frequency of Alpine glacier snout collapse. *Geophysical Research Letters* **48**(21), e2021GL096031. doi:10.1029/2021GL096031

Egli PE, Irving J and Lane SN (2021b) Characterization of subglacial marginal channels using 3-D analysis of high-density ground-penetrating radar data. *Journal of Glaciology* **67**(264), 759–772. doi:10.1017/jog.2021.26

Einstein HA (1937) Bedload transport as a probability problem. *Sedimentation* **1027**, C1–C105.

Fujita S, Matsuoka T, Ishida T, Matsuoka K and Mae S (2000) A summary of the complex dielectric permittivity of ice in the megahertz range and its applications for radar sounding of polar ice sheets. In *Physics of Ice Core Records*, Hokkaido, Japan, pp. 185–212.

GLAMOS (1880–2020) The Swiss Glaciers 1880-2018/19. Glaciological Reports No 1-140, Yearbooks of the Cryospheric Commission of the Swiss Academy of Sciences (SCNAT), published since 1964 by VAW / ETH Zurich. Technical report.

Hallet B (1979) A theoretical model of glacial abrasion. *Journal of Glaciology* **23**(89), 39–50. doi:10.3189/S0022143000029725

Hallet B (1996) Glacial quarrying: A simple theoretical model. *Annals of Glaciology* **22**, 1–8. doi:10.3189/1996AoG22-1-1-8

Hart JK and 5 others (2006) A wireless multi-sensor subglacial probe: Design and preliminary results. *Journal of Glaciology* **52**(178), 389–397. doi:10.3189/172756506781828575

Hart JK and 5 others (2019) Surface melt driven summer diurnal and winter multi-day stick-slip motion and till sedimentology. *Nature Communications* **10**(1), 1599. doi:10.1038/s41467-019-09547-6

Hashmi MAR and Brennan PV (2022) A LHCP printed cross dipole antenna for glacial environmental sensor networks. In *2022 52nd European Microwave Conference (EuMC)*, Milan, Italy: IEEE, pp. 620–623.

Hassan MA and Roy AG (2016) Coarse particle tracing in fluvial geomorphology. In *Tools in Fluvial Geomorphology*, 306–323, John Wiley & Sons.

Hassan MA, Church M and Ashworth PJ (1992) Virtual rate and mean distance of travel of individual clasts in gravel-bed channels. *Earth Surface Processes and Landforms* **17**(6), 617–627. doi:10.1002/esp.3290170607

Hassan MA, Voepel H, Schumer R, Parker G and Fraccarollo L (2013) Displacement characteristics of coarse fluvial bed sediment. *Journal of Geophysical Research: Earth Surface* **118**(1), 155–165. doi:10.1029/2012JF002374

Herman F and 8 others (2015) Erosion by an Alpine glacier. *Science* **350** (6257), 193–195. doi:10.1126/science.aab2386

Herman F, De Doncker F, Delaney I, Prasicek G and Koppes M (2021) The impact of glaciers on mountain erosion. *Nature Reviews Earth & Environment* **2**(6), 422–435. doi:10.1038/s43017-021-00165-9

Hubbard B and Glasser NF (2005) *Field Techniques in Glaciology and Glacial Geomorphology*. Chichester, England: John Wiley & Sons.

Hubbard B, Sharp MJ, Willis IC, Nielsen MK and Smart CC (1995) Borehole water-level variations and the structure of the subglacial hydrological system of Haut Glacier d'Arolla, Valais, Switzerland. *Journal of Glaciology* **41**(139), 572–583. doi:10.3189/S0022143000034894

Jaeger JM and Koppes MN (2015) The role of the cryosphere in source-to-sink systems. *Earth-Science Reviews* **153**, 43–76. doi:10.1016/j.earscirev.2015.09.011

Koppes MN and Montgomery DR (2009) The relative efficacy of fluvial and glacial erosion over modern to orogenic timescales. *Nature Geoscience* **2**(9), 644–647. doi:10.1038/ngeo616

Koppes MN and 5 others (2015) Observed latitudinal variations in erosion as a function of glacier dynamics. *Nature* **526**(7571), 100–103. doi:10.1038/nature15385

Lamarre H, MacVicar B and Roy AG (2005) Using passive integrated transponder (PIT) tags to investigate sediment transport in gravel-bed rivers. *Journal of Sedimentary Research* **75**(4), 736–741. doi:10.2110/jsr.2005.059

Lane SN and Nienow PW (2019) Decadal-scale climate forcing of Alpine glacial hydrological systems. *Water Resources Research* **55**(3), 2478–2492. doi:10.1029/2018WR024206

Lane SN, Bakker M, Gabbud C, Micheletti N and Saugy JN (2017) Sediment export, transient landscape response and catchment-scale connectivity following rapid climate warming and Alpine glacier recession. *Geomorphology* **277**, 210–227. doi:10.1016/j.geomorph.2016.02.015

Lewis C and 6 others (2015) Airborne fine-resolution UHF radar: An approach to the study of englacial reflections, firn compaction and ice attenuation rates. *Journal of Glaciology* **61**(225), 89–100. doi:10.3189/2015JoG14J089

Li C, Mo L and Zhang D (2019) Review on UHF RFID localization methods. *IEEE Journal of Radio Frequency Identification* **3**(4), 205–215. doi:10.1109/JRFID.2019.2924346

Liébault F, Bellot H, Chapuis M, Klotz S and Deschâtres M (2012) Bedload tracing in a high-sediment-load mountain stream. *Earth Surface Processes and Landforms* **37**(4), 385–399. doi:10.1002/esp.2245

Mancini D and Lane SN (2020) Changes in sediment connectivity following glacial debuttressing in an Alpine valley system. *Geomorphology* **352**, 106987. doi:10.1016/j.geomorph.2019.106987

Martinez K, Hart JK and Ong R (2004) Environmental sensor networks. *Computer* **37**(8), 50–56. doi:10.1109/MC.2004.91

Martinez K, Padhy P, Riddoch A, Ong HLR and Hart JK (2005) Glacial Environment Monitoring using Sensor Networks. In *Proceedings of the Workshop on Real-World Wireless Sensor Networks (REALWSN'05)*, Stockholm, Sweden: Association of Computing Machinery, pp. 20–21.

Miles KE and 5 others (2019) Instruments and methods: Hot-water borehole drilling at a high-elevation debris-covered glacier. *Journal of Glaciology* **65** (253), 822–832. doi:10.1017/jog.2019.49

Müller T and Miesen F (2022) Stream discharge, stage, electrical conductivity & temperature dataset from Otemma glacier forefield, Switzerland (from July 2019 to October 2021). Technical report, Zenodo.

Müller T, Lane SN and Schaefli B (2022) Towards a hydrogeomorphological understanding of proglacial catchments: An assessment of groundwater storage and release in an Alpine catchment. *Hydrology and Earth System Sciences* **26**(23), 6029–6054. doi:10.5194/hess-26-6029-2022

Olinde L and Johnson JPL (2015) Using RFID and accelerometer-embedded tracers to measure probabilities of bed load transport, step lengths, and rest times in a mountain stream. *Water Resources Research* **51**(9), 7572–7589. doi:10.1002/2014WR016120

Perolo P and 5 others (2019) Subglacial sediment production and snout marginal ice uplift during the late ablation season of a temperate valley glacier. *Earth Surface Processes and Landforms* **44**(5), 1117–1136. doi:10.1002/esp.4562

Prior-Jones MR and 12 others (2021) Cryoegg: Development and field trials of a wireless subglacial probe for deep, fast-moving ice. *Journal of Glaciology* **67**(264), 627–640. doi:10.1017/jog.2021.16

Riihimaki CA, MacGregor KR, Anderson RS, Anderson SP and Loso MG (2005) Sediment evacuation and glacial erosion rates at a small alpine glacier. *Journal of Geophysical Research: Earth Surface* **110**(F3), 1–17. doi:10.1029/2004JF000189.

Smeets C and 6 others (2012) A wireless subglacial probe for deep ice applications. *Journal of Glaciology* **58**(211), 841–848. doi:10.3189/2012JoG11J130

Sugiyama S and 5 others (2008) Hot water drilling and glaciological observations at the terminal part of Rhonegletscher, Switzerland in 2007. *Bulletin of Glaciological Research* **26**, 41–47.

Swift DA, Nienow PW and Hoey TB (2005) Basal sediment evacuation by subglacial meltwater: Suspended sediment transport from Haut Glacier d'Arolla, Switzerland. *Earth Surface Processes and Landforms* **30**(7), 867–883. doi:10.1002/esp.1197

Talalay P and 8 others (2018) Shallow hot-water ice drill: Estimation of drilling parameters and testing. *Cold Regions Science and Technology* **155**, 11–19. doi:10.1016/j.coldregions.2018.07.006

Tsutaki S and Sugiyama S (2009) Development of a hot water drilling system for subglacial and englacial measurements. *Bulletin of Glaciological Research* **27**, 7–14.